PREPARATION AND CHARACTERISATION OF A NEW STAINLESS STEEL/Bi$_2$O$_3$ ANODE AND ITS DYES DEGRADATION ABILITY

Milica M. Petrović,* Jelena Z. Mitrović, Miljana D. Radović, Miloš M. Kostić and Aleksandar L. J. Bojić

Department of Chemistry, Faculty of Science and Mathematics, University of Niš, Niš, Višegradska 33 18000, Serbia

Stainless steel/Bi$_2$O$_3$ anode was synthesised by electrodeposition from acidic Bi (III) solution on stainless steel substrate and calcination at 500°C. Characterisation by SEM, EDX, XRD and TGA revealed that the anode surface was fully covered with pure α-Bi$_2$O$_3$, which formed a inhomogeneous and porous coat. Three dyes with different chromophores, namely: Reactive Blue 19, Methylene blue and Reactive Orange 4 were completely decolourised by electrochemical oxidation at the synthesised anode in the presence of hydrogen peroxide. Decolourisation followed the pseudo-first order kinetics model for all the three dyes. Decolourisation rates are sorted in descending order: Reactive Orange 4 > Reactive Blue 19 > Methylene Blue. For all the three dyes, an increase of the initial dye concentration caused the decrease of the reaction rate constants. At higher initial dye concentrations, the decolourisation times were significantly prolonged for all the three dyes, however, the complete decolourisation was done as well.

Keywords: Bi$_2$O$_3$, anode, dyes, decolourisation

INTRODUCTION

Electrochemical oxidation has been largely developed for removing organic pollutants from aqueous solutions, including synthetic organic dyes. The oxidation of pollutants can be done as the direct anodic oxidation, or as a chemical reaction with electrogenerated species from water discharge at the anode surface such as "active oxygen," that is hydroxyl radical •OH. This radical is a very strong oxidant, with a high standard potential ($E_0 = 2.80$ V vs. SHE) that ensures its fast reaction with most organics, and it is considered the responsible species for the electrochemical oxidative degradation of organic pollutants.[1] Anode material is a very important factor in the processes of electrochemical decolourisation. Anodes based on metal oxides have a high surface area and an excellent mechanical and chemical resistance even at high current densities. Various materials based on metal oxides, such as PbO$_2$, RuO$_2$, IrO$_2$, SnO$_2$, SbO$_x$, etc. and their mixtures have been used for electrochemical degradation of dyes, showing various colour removal efficiency.[1–11] Some semiconductor metal oxide based anodes are used in photo-electrocatalytic oxidation processes.[1]

Bismuth oxide (Bi$_2$O$_3$) is an important transition metal oxide which has been recently applied as a photocatalyst in the processes of the removal of various compounds, including gaseous NO and HCHO,[12] Rhodamine B,[13] Methyl Orange and 4-chlorophenol,[14] dye Acid Orange 7,[15] etc. Bi$_2$O$_3$ and Au–Bi$_2$O$_3$ nanoparticles were successfully applied in catalytic ozonation of Acid Orange 10.[16] Microcrystalline Bi$_2$O$_3$ can offer a large surface area, electrochemical stability and catalysis behaviour which makes it an interesting material for electrochemical oxidation of various organic pollutants. Bi$_2$O$_3$ microparticles deposited onto glassy carbon electrode were successfully applied as the electrocatalyst in the process of electrochemical oxidation of ascorbic acid.[17] The Bi$_2$O$_3$/Ti electrode was used in oxidative degradation of Acid Orange 7 by electrolysis, photocatalytic oxidation and photo-electrocatalytic oxidation processes.[15]

Bi$_2$O$_3$ is relatively easy to prepare and the precursors are generally low cost. Various synthesis routes have been developed and applied. Some of these routes are: precipitation from alkaline Bi (III) solutions,[14,18] sol–gel aqueous procedure and modified sol–gel procedure, based on the esterification reaction,[19,20] microwave-assisted method,[21] thermal oxidation of bismuth nanoparticles,[22] atmospheric pressure chemical vapour deposition[23] and electrochemical deposition or electrodeposition under various experimental conditions. Bi$_2$O$_3$ films and powders have been successfully electrodeposited from acidic and alkaline Bi(III) solutions, on various conductive substrates, including Ti, stainless steel, Cu, Au, Ag, etc.[15,24–27] Electrodeposition is a very convenient method of material synthesis, because it is simple and it offers rigid control of film thickness, uniformity, and deposition rate and is especially attractive because of its low equipment cost and starting materials. In cathodic electrodeposition, metal ions or complexes are hydrolysed by electrogenerated OH$^-$ ions to form oxide, hydroxide, or peroxide deposits on cathodic substrates. Hydroxide and peroxide deposits can be converted to corresponding oxides by thermal treatment.[28] Bi$_2$O$_3$ can also be obtained by bismuth film electrodeposition on a conductive substrate, followed by its anodisation.[29]

In this work, Bi$_2$O$_3$-based anode was synthesised by Bi electrodeposition from acidic solution on stainless steel substrate at constant potential, using a chronoamperometric technique, followed by calcination. The aim of the work was to investigate the properties of the obtained anode and its ability to degrade thiazine dye Methylene blue, anthraquinone reactive dye Reactive Blue 19 (RB 19) and triazine azo reactive dye Reactive Orange 4 (RO 4) by electrochemical oxidation in the presence of H$_2$O$_2$.

EXPERIMENTAL

Materials

Bismuth (III) nitrate pentahydrate, nitric acid, hydrogen peroxide, sodium sulphate and Methylene blue were of reagent grade and used without further purification. Reactive Blue 19 and Reactive Orange 4 were obtained from Farbotex (Italy) and used without further purification. All solutions were prepared by deionised water.

Preparation of the Anodes

All electrochemical experiments were carried out using Amel 510 DC potentiostat (Materials Mates, Milano, Italy) furnished with VoltaScope software package. Electrodeposition was performed at $20 \pm 0.5°C$ in the three electrode cell with a stainless steel sheet (10×25 mm) as a substrate (cathode), a Pt sheet (10×20 mm) as auxillary electrode (anode), and saturated calomel electrode (Materials Mates) as a reference electrode. Note that, for the convenience, the potentials are calculated and given versus the standard hydrogen electrode (SHE). The distance between the working and auxillary electrode was 15 mm. Before the electrodeposition, the substrate was polished with different abrasive papers, ultrasonically cleaned with acetone and deionised water, anodically treated in 0.5 M oxalic acid at a current density of 500 mA cm^{-2} and finally washed with deionised water. An electrodeposition solution of 0.1 M Bi^{3+} was prepared by dissolving the required amount of bismuth nitrate in 1 M HNO$_3$ water solution. Electrodeposition was carried out at a constant potential of 0.6 V during 3 min, using a chronoamperometric technique. After the deposition, the substrate covered with deposited film was washed with water, dried at room temperature for 24 h, calcined at 500°C for 90 min in air in a furnace and cooled in the open air.

Characterisation of the Obtained Anode

Surface morphology of the anode was investigated by a scanning electron microscopy (SEM) technique. Samples were stuck onto aluminium stubs using Leit-C carbon cement and then carbon coated in an Edwards 306 high vacuum carbon evaporator to ensure surface conductivity for EDX. Secondary electron images were taken using the lower detector of a Hitachi SU8030 cold-cathode field emission gun scanning electron microscope (FEG-SEM) at 2 kV accelerating voltage, at various working distances between 10 and 16 mm and at nominal magnifications of $150\times$, $1000\times$ and $5000\times$. Energy Dispersive X-ray microanalysis (EDX) was performed using a Thermo-Noran NSS system 7 with a 30 mm^2 window Ultra Dry detector. The working distance was fixed at 15 mm and an accelerating voltage of 10 kV was chosen to give adequate excitation of the K lines of the lighter elements, the L lines of Cu, Cd and Ni, and the M lines of Bi and Pb while limiting the beam damage to the sample. Three replicate analyses were taken within a single field of view. TGA studies were performed using TGA Q5000 (TA Instruments, New Castle, DE). For this purpose, another anode was prepared in exactly the same way as the one for the dye degradation experiments and a small sample of Bi$_2$O$_3$ was carefully peeled. The sample mass used was 2.00 ± 0.50 mg. The sample was heated in air at a flow rate of 25 mL/min from ambient temperature to 600°C in aluminium pan, at a heating rate of 10°C/min. An x-ray diffraction (XRD) pattern was taken by the use of a Siemens D500 diffractometer (Munich, Germany) with a Ni filter using Cu Kα radiation ($\lambda = 0.154$ nm) and the step-scan mode with a step width of $0.02°$ and 1 s/step.

Dyes Decolourisation Experiments

Dyes decolourisation experiments were carried out at a temperature of $20 \pm 0.5°C$ (which was held constant during the experiments) in a three-electrode cell, at various initial dye concentrations, with Pt sheet as the cathode. The applied current density was 40 mA cm^{-2} in all the experiments. RB19, Methylene blue and RO 4 solutions of 0.02, 0.04, 0.08, 0.16 and 0.32 mmol dm^{-3} of the dye, 10 mmol dm^{-3} H$_2$O$_2$ and 10 mmol dm^{-3} Na$_2$SO$_4$ were prepared separately by dissolving the proper amounts of powdered dye, H$_2$O$_2$ and Na$_2$SO$_4$ in water; pH of all the solutions was 7 ± 0.1 During the decolourisation experiments, the dye solutions were stirred on a magnetic stirrer. The in situ anode potential was in the range of about 2.8 V. The dye concentrations were determined using UV–vis spectrophotometer Shimadzu UV-1650 PC (Shimadzu, Kyoto, Japan). The percentage of decolourisation was calculated using the equation:

$$\text{Percentage of decolorization} (\%) = \frac{c_0 - c_t}{c_0} \times 100 \qquad (1)$$

where c_0 is the initial dye concentration and c_t is the dye concentration at the time t.

RESULTS AND DISCUSSION

Electrodeposition was performed at a constant cathodic potential. The aim was to obtain mechanically and electrochemically stable Bi$_2$O$_3$ thin film in the shortest possible time. Electrodeposition conditions affected the film's quality and the applied cathodic potential had the most significant influence. Preliminary investigation has shown that the films obtained at lower cathodic potentials (0.40 and 0.50 V) were formed faster than those obtained at higher potentials, because the current density at lower potentials was higher. However, those films were not mechanically stable enough. The increase of the deposition potential to 0.60 V provided mechanically stable films. Further increase of the deposition potential did not significantly improve the film's quality, and the deposition time needed to cover the entire metallic surface was significantly prolonged. Thus, based on these investigations, the working electrode potential of 0.60 V was selected as the optimal for electrodeposition. The film obtained at this potential was mechanically stable and it was obtained during 3 min. The variations of current density (j) during the deposition at 0.60 V are shown in Figure 1. The value of the starting current density was little more than 45 mA cm^{-2}, and it slowly increased during the given time interval up to about 58 mA cm^{-2}, but no significant
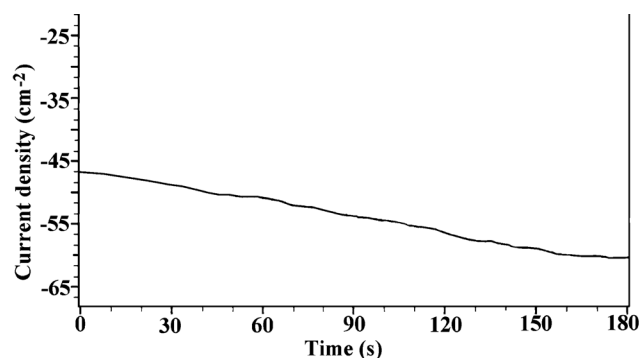

Figure 1. Dependence of current density on deposition time at constant potential of 0.6 V in acidic nitrate 0.1M Bi^{3+} solution.

changes in the corresponding curve's shape were observed (Figure 1).

The colour of the deposited material was grey. Bi may exist in several soluble forms, depending on the solution pH.[24–27,30] For the H$^+$ ions concentration >0.4 M, which is the case in our work, the aqua Bi^{3+} prevails, and the predominant cathodic reaction may be[30]:

$$Bi^{3+} + 3e^- \rightarrow Bi^0 \tag{2}$$

The presence of the predominant metallic Bi at the substrate surface was confirmed by EDX analysis, which showed that before the calcination, the molar ratios of Bi and O on the surface were 94.20% and 5.80%, respectively (i.e. corresponding weight ratios were 99.53% and 0.47%, respectively; spectrum not shown). After the calcinations at 500°C, the colour of the deposited material changed to pale yellow, indicating that the Bi$_2$O$_3$ was formed.

Characterisation

SEM images

The surface morphology of the calcined stainless steel/Bi$_2$O$_3$ anode is presented in Figure 2.

The metallic surface is fully covered with the Bi$_2$O$_3$ coating (Figure 2a). The surface is not uniform and homogeneous. It is rather composed of small aggregates, which are not packed very closely forming a uniform structure, but rather rough, porous surface with a higher area than the homogeneous, compact structure would offer. At higher magnifications, a great variety in size and morphology of the Bi$_2$O$_3$ particles can be observed, with a lot of particles less than 1 μm in diameter attached to the much bigger aggregates (Figure 2b,c). On some parts of the surface, it is hard to distinguish whether some parts are compact large particles (larger than 10 μm), or aggregates composed of closely packed smaller particles. The shapes of the particles vary a lot. They are random and mainly irregular, and many of them have pores of different size. In general, the two types of particles can be observed: the small, oval, closely packed particles, which form the large, relatively compact aggregates, and the larger ones, with the sharp edges and irregular shapes (Figure 2b,c). Such a variety of the particles size and shape is probably the consequence of the current changes during the electrodepositon and of the fact that the formation of the particles and their attachment to the surface proceeded relatively rapidly, due to a relatively high current density. The thickness of Bi$_2$O$_3$ film, obtained by scanning the anode cross section (picture not shown) by SEM, is 15 ± 5 μm.
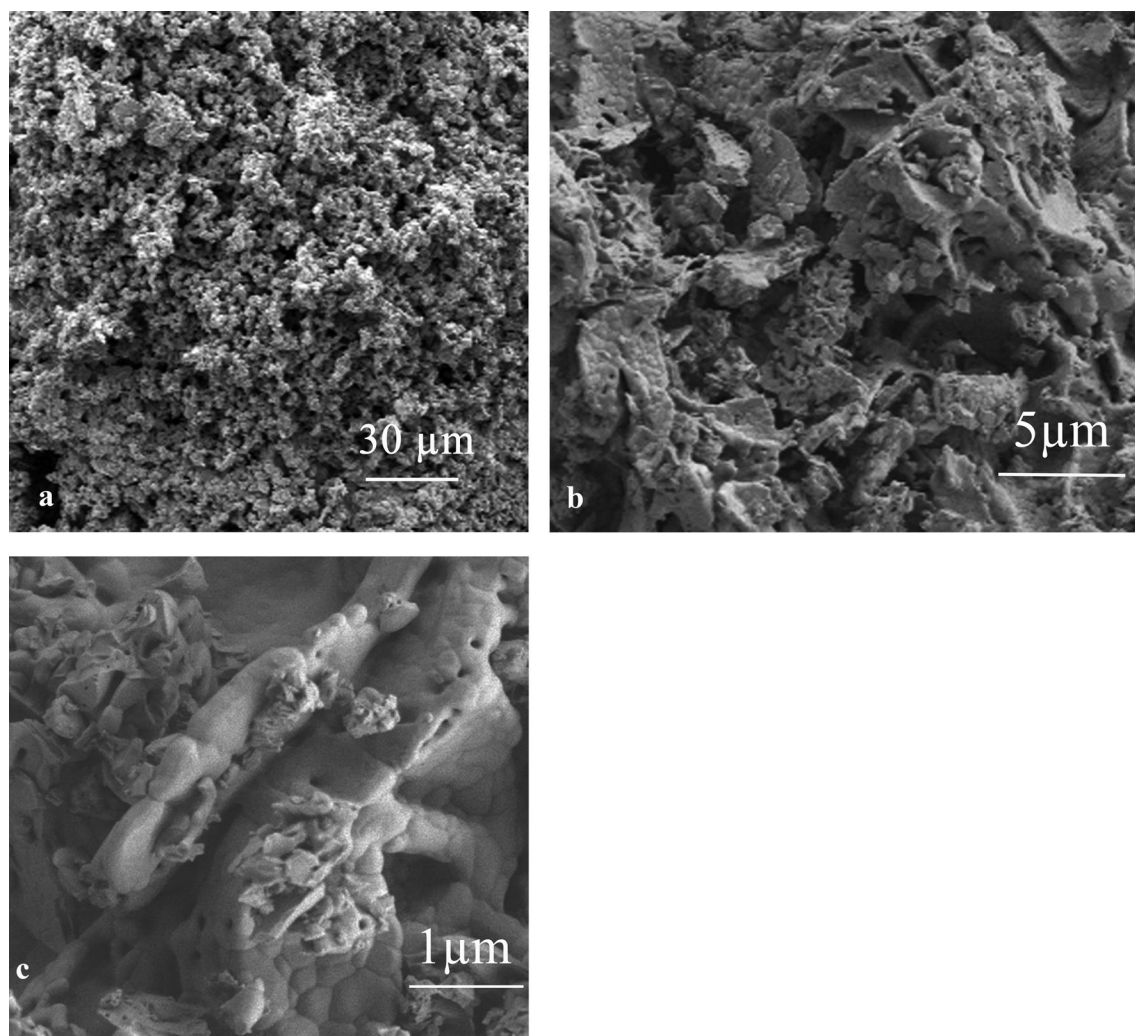
Figure 2. SEM images of stainless steel/Bi$_2$O$_3$ anode obtained by electrodeposition from Bi^{3+} acidic solution and calcination at 500°C with magnifications: (a) 150×, (b) 1000× and (c) 5000×.

Before the dye degradation experiments were started, the anode has been repeatedly exposed to high potentials, at which the dye degradation experiments were performed, in the presence of H_2O_2, during several hours. After those tests, neither change in the anode mass, nor the presence of bismuth in the solutions was detected. This indicates that the Bi_2O_3 layer is very well adhered to the surface and the obtained anode is mechanically and electrochemically stable under the applied dye degradation conditions. The anode's surface is large and porous, which offers a lot of space for the formation of a higher concentration of •OH radicals from aqueous peroxide solutions (Table 1).

EDX spectrum analysis

Figure 3 shows well defined peaks for Bi and O elements, confirming the presence of Bi_2O_3 (note that the spectrum is drawn based on the weight percentage of the elements on the surface, but their molar ratios are numerically given, due to easier comparison). The molar ratios of Bi and O on the examined surface are 36.08% and 63.92%, respectively, which are close enough to the theoretical values of Bi and O molar ratio in Bi_2O_3 of 40% and 60%, respectively (i.e. corresponding weight ratios are 88.05% and 11.95%, respectively, close to their theoretical weight ratios in Bi_2O_3 of 89.70% and 10.30%, respectively), indicating that the prepared electrode is coated with practically pure Bi_2O_3.

The obtained results, which show a little lower content of Bi and little higher content of O than theoretical, are somewhat different than those obtained by Salazar-Pérez et al.,[22] who reported that bismuth oxide obtained at temperatures between 500 and 750°C had a little higher, and that obtained at about 400°C had a little lower content of Bi than theoretical.

TG analysis

Figure 4 shows TG results for the deposit which was mechanically stripped from the stainless steel substrate surface after the calcination at 500°C and cooling to the room temperature.

The obtained Bi_2O_3 powder was heated from room temperature to 600°C at a heating rate of 10°C/min. No significant change of its weight was observed within the given temperature interval,
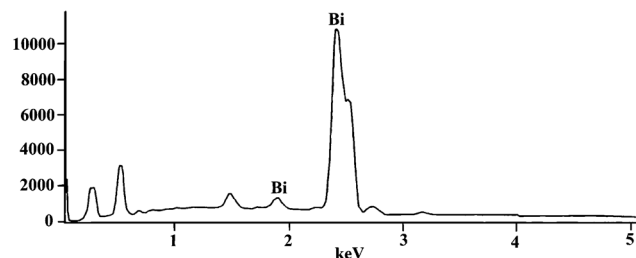

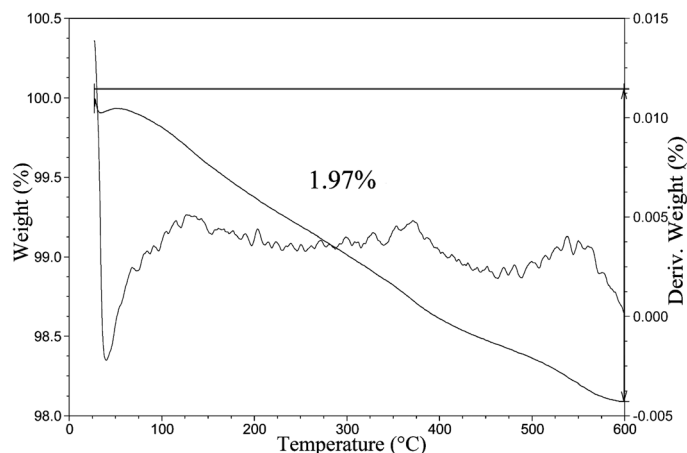**Figure 3**. EDX analysis spectra of stainless steel/Bi_2O_3 anode.
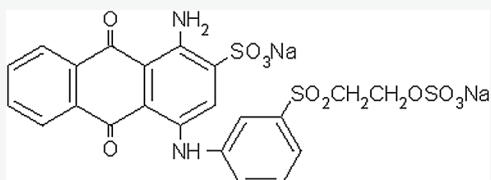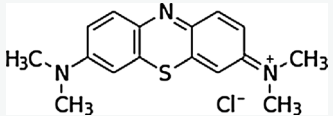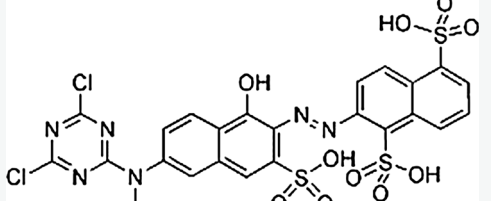

Figure 4. TG data for deposit obtained by electrodeposition from 0.1 M Bi^{3+} acidic solution, fallowed by calcination at 500°C.

indicating that the obtained material is chemically stable under those conditions. The total weight loss was 1.97% and it proceeded almost linearly in the heating range. A little more significant weight loss was observed when the temperature exceeded 500°C. This might be attributed to a slight loss of oxygen; as mentioned above, Bi_2O_3 obtained in the range of 500–750°C was oxygen deficient.[22] However, there was no change in the shape of the derivative weight

Table 1. Main characteristics of the dyes used			
Dye	Chemical structure	IUPAC name	Molar mass (g mol^{-1})
Reactive blue 19		2-(3-(4-Amino-9,10-dihydro-3-sulpho-9, 10-dioxoanthracen-4-yl) aminobenzenesulphonyl)vinyl) disodium sulphate	626.54
Methylene blue		3,7-bis(Dimethylamino)-phenothiazin-5-ium chloride	319.85
Reactive orange 4		1,5-Naphthalenedisulfonic acid, 2-[[6-[(4,6-dichloro-1,3,5-triazin-2-yl) methylamino]-1-hydroxy-3-sulfo -2- naphthalenyl]azo]-, trisodium salt	715.53

loss curve that might be caused by some chemical reaction, indicating that the obtained material is stable in the examined temperature range which is further support for the presence of pure Bi_2O_3.

XRD spectrum analysis

X-Ray diffraction (XRD) was used to reveal the phase structure of the obtained Bi_2O_3.

Sharp, narrow, well defined diffraction peaks indicate the high crystallinity of the obtained material. Bi_2O_3 is known to exist in several polymorphous modifications: monoclinic α-Bi_2O_3, stable at room temperature; cubic fluorite type δ-Bi_2O_3 which exists above 729°C up to a melting point of 825°C; and two metastable phases, which may occur upon cooling near 650 and 640°C, respectively: the tetragonal β-phase, and body-centred cubic γ-phase. They usually transform to α-phase upon further cooling to the room temperature.[14,20,31] A series of diffraction peaks with characteristic 2θ values at: 27.4°, 33.3° and 46.3°, corresponding to (120), (200) and (041) reflection, respectively, can be attributed to monoclinic α-Bi_2O_3. No trace of any other Bi_2O_3 phase was detected (Figure 5). A synthesis route has much effect on the crystalline structure of the final product[13,14,20,31,32] and temperature is an important factor determining that structure. In this work, electrodeposited material was thermally treated at 500°C, which lead to a formation of pure α phase. This result is generally in accordance with those reported in the literature where at the temperatures of 500°C and higher, the formation of α-Bi_2O_3 prevails.[12,20,22] However, Wang et al.[13] reported that calcination at 500°C produced β-Bi_2O_3, while calcination at 550–600°C produced β phase with traces of α phase. This indicates that not only the temperature, but the whole synthesis route affects the crystalline structure of the obtained product, although the temperature is the most important factor. In general, α phase is formed at higher heating temperatures. The formation of α-phase was also observed when the thermal treatment at 400°C was prolonged from 1 to 4 h.[20]

It should be noted that no traces of the presence of iron-oxide were detected on the examined anodes surface.

Dyes decolourisation

The effect of H_2O_2 alone, electric current without H_2O_2, and electric current plus H_2O_2 was examined. The solutions of RB 19, MB and RO 4 (0.08 mmol dm^{-3}) and 10 mmol dm^{-3} H_2O_2 were left in the dark and in the light for 48 h and the dye removal efficiency was negligible for all the three dyes (resu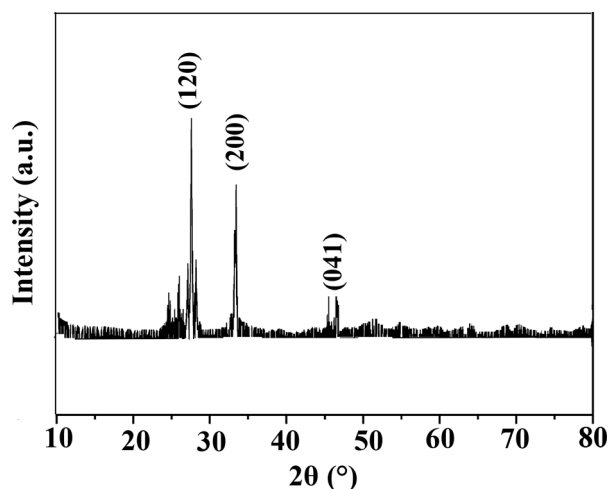lts not shown). Electrolysis of the dyes solutions in the absence of H_2O_2 at the constant current density of 40 mA cm^{-2} also gave poor decolourisation; only 5%, 1% and 11% of RB 19, MB and RO 4, respectively, were removed within 2 h. This removal probably proceeded through a direct anodic oxidation of the dyes, which is generally a slow reaction, due to a high stability of the synthetic organic dyes molecules.[1] The other possibility is indirect oxidation of the dyes by "active oxygen" produced from water discharge at the anode, which is also a slow reaction, because the production of hydroxyl radicals electrochemically generated with water is small during indirect oxidation. Therefore, a long reaction time or a high current density is usually required to achieve satisfactory colour removal.[32] However, when the constant current density of 40 mA cm^{-2} was applied in the presence of H_2O_2, a much faster colour removal was observed. RB 19, MB and RO 4 were completely removed in about 65, 125 and 35 min, respectively, with the 37.5%, 15.1% and 64.8% dye removal in the first 5 min of electrolysis (Figure 6). This removal can be related to an indirect electrochemical oxidation of the dyes by highly reactive species, electrogenerated from H_2O_2 decomposition at high potentials, such as hydroxyl radical •OH.[1,33] The increase in the initial H_2O_2 concentration caused the increase of •OH radical concentration in the solution and thus, the increase in decolourisation rates (results not shown), but only up to 10 mmol dm^{-3}. Further increase in H_2O_2 concentration slightly decreased the dyes decolourisation rates, probably because of quenching reaction of hydroxyl radicals with H_2O_2[32]:

$$H_2O_2 + \bullet OH \rightarrow HO_2\bullet + HO_2 \qquad (3)$$

The generated hydroperoxyl radical $HO_2\bullet$ is less reactive than H_2O_2 and it could not oxidise the dyes. So, the optimal H_2O_2 concentration was found to be 10 mmol dm^{-3} in the case of all the three dyes and it was applied in all the experiments.

All the three dyes, which have different molecular structures and chromophores, could be completely removed by indirect oxidation at the synthesised Bi_2O_3 anode. Dyes decolourisation rates were different. The fastest decolourisation was achieved for RO 4, that for RB 19 was significantly slower, and the slowest decolourisation was observed for MB. These differences are related to the different structures and chromophores, and thus, the stability of the dyes molecules.[34] It should be noted that no detectable adsorption of
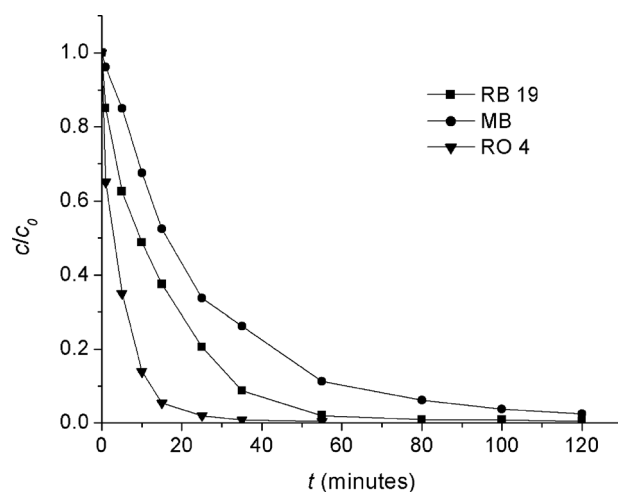

Figure 5. XRD pattern of synthesised Bi_2O_3.

Figure 6. Effect of time on the decolourisation of RB 19, MB and RO 4 (c_0 (RB 19) = c_0 (MB) = c_0 (RO 4) = 0.08 mmol dm^{-3}, c_i (H_2O_2) = 10 mmol dm^{-3}, c_i (Na$_2$SO$_4$) = 10 mmol dm^{-3}, current density 40 mA cm^{-2}, pH 7.0 ± 0.2, temperature 20 ± 0.5°C).

RB 19 and RO 4 on the surface of the anode took place under the reaction conditions applied in the electrochemical experiments described in this paper. The adsorption of MB was negligible.
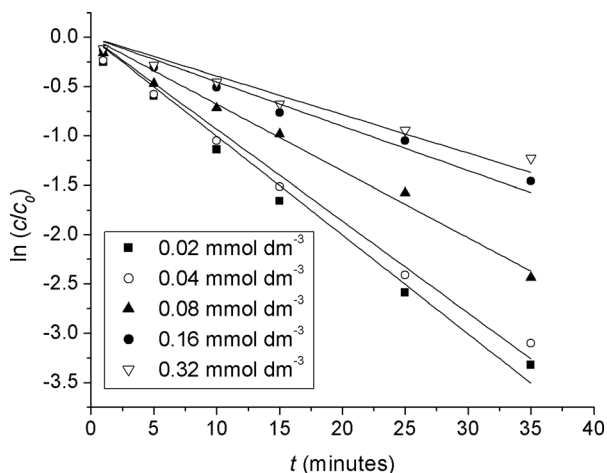
Initial dye concentration (c_0) is a very important factor for an electrochemical dye removal process. In order to investigate its effect on the decolourisation rate, electrolysis was performed at various initial dye concentrations. The results are shown in Figures 7–9, where ln (c/c_0) values are plotted against time scale; c_0 is initial dye concentration and c is a dye concentration after reaction time t.

For all the three dyes, for all of the tested initial dye concentrations, ln (c/c_0) practically linearly decreases as the reaction time increases, meaning that the reactions can be well described by means of the pseudo-first order kinetics model:

$$\ln\left(\frac{c}{c_0}\right) = -kt \qquad (4)$$

where k is the reaction rate constant ($\min^{-1}$). The result is in accordance with those reported in literature for the advanced oxidation processes of organic molecules, in which those molecules are oxidised by strong oxidants, generated by electric power source, UV irradiation, photocatalysis, etc.[15,35–42] This further supports the indirect oxidation of the dyes by hydroxyl radical •OH, electrogenerated at the Bi_2O_3 anode surface.

The initial dye concentration has a significant impact on the dyes decolourisation rate. The removal of RB19 in the first 5 min was: 45.1%, 44.0%, 37.5%, 26.5% and 24.7% for: 0.02, 0.04, 0.08, 0.16 and 0.32 mmol dm^{-3} of the dye, respectively (Figure 7). Total decolourisation times for: 0.02, 0.04, 0.08, 0.16 and 0.32 mmol dm^{-3} of the dye are: 45, 48, 65, 104, and 120 min, respectively, corresponding reaction rate constants are: 0.1002, 0.0931, 0.0678, 0.04340 and 0.0376, respectively, and the corresponding values of the square of the relative correlation coefficients R^2 are: 0.9938, 0.9944, 0.9947, 0.9888 and 0.9843, respectively. As it can be observed, RB 19 decolourisation rate decreases as the initial dye concentration increases; at low initial dye concentrations, c_0 does not have much impact on the decolourisation rate constant; increasing c_0 from 0.02 to 0.04 mmol dm^{-3}, decreased the reaction rate by only 7.08%. A much more significant decrease of k was observed by increasing c_0 from 0.04 to 0.08 mmol dm^{-3} and it was 37.32%. Increasing c_0 from 0.08 to

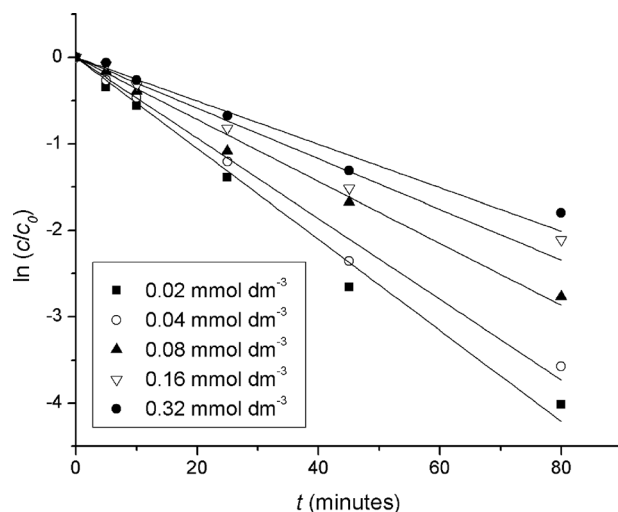0.16 mmol dm^{-3} decreased the reaction rate by 56.22%, which was the most significant decrease of the RB 19 decolourisation rate for the investigated c_0 range. Further increase of c_0 to 0.32 mmol dm^{-3} did not bring such a significant decrease in the reaction rate as it was observed at lower initial dye concentrations; the reaction was slower by 15.42% related to that of 0.32 mmol dm^{-3}.

Decolourisation of MB proceeded slower than that of RB 19, meaning that the corresponding decolourisation rate constants are lower than those of RB 19. The removal of MB in the first 5 min was: 42.9, 33.1, 32.5, 26.7 and 22.9% for: 0.02, 0.04, 0.08, 0.16 and 0.32 mmol dm^{-3}, respectively (Figure 8). Total decolourisation times for: 0.02, 0.04, 0.08, 0.16 and 0.32 mmol dm^{-3} of the dye are: 85, 96, 125, 157 and 185 min, respectively, the corresponding reaction rate constants are: 0.0526, 0.0466, 0.0359, 0.0284 and 0.0242, respectively, and the corresponding values of the square of the relative correlation coefficients R^2 are: 0.9937, 0.9945, 0.9949, 0.9835 and 0.9826, respectively. MB decolourisation rate decreases as the initial dye concentration increases in the similar way as in the case of RB 19; at low initial dye concentrations, c_0 does not have much impact on the decolourisation rate constant, however that impact is bigger than in the case of RB 19; increasing c_0 from 0.02 to 0.04 mmol dm^{-3} decreased the reaction rate by 12.88%, and a more significant decrease of k was observed by increasing c_0 from 0.04 to 0.08 mmol dm^{-3} and it was 29.81%, which was the most significant decrease of the RB 19 decolourisation rate for the investigated c_0 range. Increasing c_0 from 0.08 to 0.16 mmol dm^{-3} decreased the reaction rate by 26.41%. Further increase of c_0 to 0.32 mmol dm^{-3} did not bring such a significant decrease in the reaction rate as it was observed at lower initial dye concentrations; the reaction was slower by 17.36% related to that of 0.32 mmol dm^{-3}.

The fastest decolourisation was observed in the case of RO 4. The removal of dye in the first 5 min was: 70.1%, 68.0%, 64.9%, 54.2% and 49.1% for: 0.02, 0.04, 0.08, 0.16 and 0.32 mmol dm^{-3}, respectively (Figure 9). Total decolourisation times for: 0.02, 0.04, 0.08, 0.16 and 0.32 mmol dm^{-3} of the dye are: 27, 28, 30, 40 and 45 min, respectively, corresponding reaction rate constants are: 0.2035, 0.1937, 0.1755, 0.1337 and 0.1241, respectively, and the corresponding values of the square of the relative correlation coefficients R^2 are: 0.9906, 0.9916, 0.9901, 0.9861 and 0.9878, respectively. RO 4 decolourisation rate decreases as the initial dye

Figure 7. Effect of initial dye concentration on the decolourisation rate of RB 19 (c_i (H$_2$O$_2$) = 10 mmol dm^{-3}, c_i (Na$_2$SO$_4$) = 10 mmol dm^{-3}, current density 40 mA cm^{-2}, pH 7.0 ± 0.2, temperature 20 ± 0.5°C).

Figure 8. Effect of initial dye concentration on the decolourisation rate of MB (c_i (H$_2$O$_2$) = 10 mmol dm^{-3}, c_i (Na$_2$SO$_4$) = 10 mmol dm^{-3}, current density 40 mA cm^{-2}, pH 7.0 ± 0.2, temperature 20 ± 0.5°C).
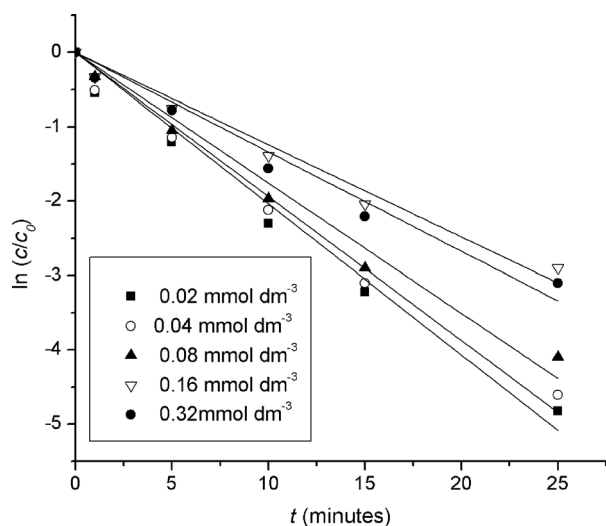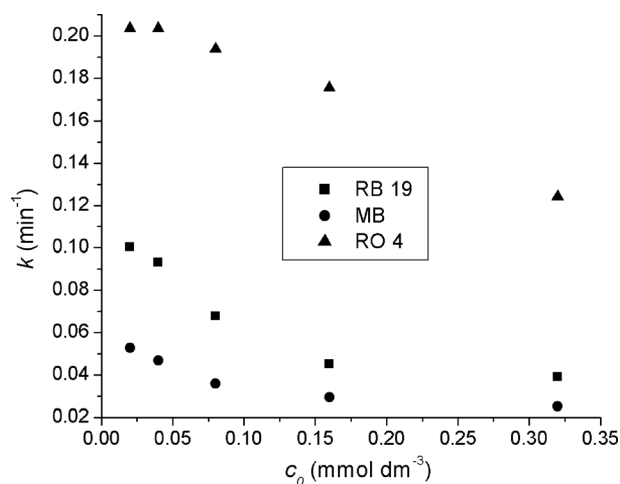
Figure 9. Effect of initial dye concentration on the decolourisation rate of RO 4 (c_i (H_2O_2) = 10 mmol dm^{-3}, c_i (Na_2SO_4) = 10 mmol dm^{-3}, current density 40 mA cm^{-2}, pH 7.0 ± 0.2, temperature 20 ± 0.5°C).

Figure 10. Effect of initial dye concentration on the rate constant of the dyes decolourisation (c_0 (H_2O_2) = 10 mmol dm^{-3}, c_0 (Na_2SO_4) = 10 mmol dm^{-3}, current density 40 mA cm^{-2}, pH 7.0 ± 0.2, temperature 20 ± 0.5°C.

concentration increases in the similar way as in the case of RB 19 and MB. At low initial dye concentrations, c_0 does not have much impact on the decolourisation rate constant; increasing c_0 from 0.02 to 0.04 mmol dm^{-3}, decreased the reaction rate by only 5.06% and a much more significant decrease of k was observed by increasing c_0 from 0.04 to 0.08 mmol dm^{-3} and it was 10.37%. Increasing c_0 from 0.08 to 0.16 mmol dm^{-3} decreased the reaction rate by 31.26%, which was the most significant decrease of the RB 19 decolourisation rate for the investigated c_0 range. Further increase of c_0 to 0.32 mmol dm^{-3} did not bring such a significant decrease of the reaction rate as it was observed at lower initial dye concentrations; the reaction rate constant was lower by only 7.74% related to that of 0.32 mmol dm^{-3}.

In general, decolourisation rates of the dyes can be sorted in descending order: triazine azo dye RO 4 > anthraquinone dye RB 19 > thiazine dye MB. The differences between the dyes decolourisation rates are attributed to a presence of different chromophores in their molecules, which have different stabilities toward oxidation under the conditions applied in this work. Decolourisation rate constants decrease with increasing initial dye concentration in the investigated concentration range for all the three dyes. In the case of RB 19 and RO 4, c_0 has a relatively low effect on the dye decolourisation rate at low c_0 values, and that effect is a little higher for MB. As expected, at higher initial dye concentrations, the decolourisation rate significantly decreases with increasing c_0 for all the three dyes (Figure 10), probably because the ratio between the dye and •OH radical concentration increases, decreasing the amount of •OH available for the reaction with the dye molecules, thus prolonging the decolourisation reaction time.[39,40] All the decolourisation reactions followed the pseudo-first order kinetics model, with the R^2 values higher than 0.99 for c_0 = 0.02, 0.04 and 0.08 mmol dm^{-3}, and than 0.98 for c_0 = 0.16 and 0.32 mmol dm^{-3}.

Though the decolourisation times are significantly prolonged for c_0 = 0.16 and 0.32 mmol dm^{-3}, the complete decolourisation of all the tested dyes using steel/Bi$_2$O$_3$ anode is possible under the applied experimental conditions. The fact that the compounds with different structures were completely decolourised at the anode surface and that all the reactions followed the pseudo-first order kinetics, a characteristic for the advanced oxidation processes

where compounds are oxidised by hydroxyl radical •OH, indicated that there were no specific reactions between the dyes and the anode during the decolourisation process, that is decolourisation proceeded through oxidation by hydroxyl radical •OH, electro-generated at the anode.

CONCLUSIONS

- A stainless steel/Bi$_2$O$_3$ anode was synthesised by electrodeposition on stainless steel from Bi (III) acidic solution at constant potential, followed by calcination at 500°C. The anode surface was covered with pure α-Bi$_2$O$_3$ particles of different and irregular shapes and sizes, making it inhomogeneous and porous. The molar ratios of Bi and O on the examined surface were found to be 36.08% and 63.92%, respectively. TG analysis revealed that the obtained Bi$_2$O$_3$ was chemically stable in the heating temperature range, that is up to 600°C.

- Solutions of anthraquinone dye Reactive Blue 19, thiazine dye Methylene blue and triazine azo dye reactive Orange 4 were completely decolourised by electrochemical oxidation at the synthesised anode in the presence of hydrogen peroxide. The oxidation was done with anodically generated hydroxyl radical •OH. All the decolourisation reactions followed the pseudo-first order kinetics model. Dyes decolourisation rates are sorted in descending order: Reactive Orange 4 > Reactive Blue19 > Methylene Blue. The differences of the decolourisation rate constants are attributed to the different structures of the dyes molecules.

- Initial dye concentration affected the dyes decolourisation rate. For all the three dyes, an increase of the initial dye concentration caused the decrease of the reaction rate constants. At higher initial dye concentrations, the decolourisation times were significantly prolonged for all the three dyes, however, the complete decolourisation was done as well.

- The synthesised stainless steel/Bi$_2$O$_3$ anode is prepared relatively fast and easily, using the low-cost and simple equipment and the low-cost materials; it has demonstrated good decolourisation ability for the three entirely different dyes with different molecular structures and chromophores, which makes it a promising material for further investigation and

application in harmful organic compounds removal from water.

REFERENCES

[1] C. A. Martínez-Huitle, E. Brillas, *Appl. Catal. B* **2009**, *87*, 105.

[2] J. L. Nava, M. A. Quiroz, C. A. Martínez-Huitle, *J. Mex. Chem. Soc.* **2008**, *52*, 249.

[3] J. M. Aquino, R. C. Rocha-Filho, N. Bocchi, S. R. Biaggio, *J. Braz. Chem. Soc.* **2010**, *21*, 324.

[4] R. F. Yunus, Y. Zheng, K. G. N. Nanayakkara, J. P. Chen, *Ind. Eng. Chem. Res.* **2009**, *48*, 7466.

[5] K. Wang, M. Wei, T. Peng, H. Li, S. Chao, T. Hsu, H. Lee, S. Chang, *J. Environ. Manage.* **2010**, *91*, 1778.

[6] P. A. Carneiro, C. S. Fugivara, R. F. P. Nogueira, N. Boralle, M. V. B. Zanoni, *Portugaliae Elchem. Acta* **2003**, *21*, 49.

[7] M. Ihos, F. Manea, A. Iovi, *Chem. Bull. "Politehnica"* **2009**, *54*, 46.

[8] M. Hamza, R. Abdelhedi, E. Brillas, I. Sirés, *J. Electroanal. Chem.* **2009**, *627*, 41.

[9] M. Muthukumar, M. Thalamadai, G. Karuppiah, R. Bhaskar, *Sep. Purif. Technol.* **2007**, *55*, 198.

[10] X. Chen, F. Gao, G. Chen, *J. Appl. Electrochem.* **2005**, *35*, 185.

[11] G. B. Raju, M. T. Karuppiah, S. S. Latha, D. L. Priya, S. Parvathy, S. Prabhakar, *Desalination* **2009**, *249*, 167.

[12] Z. Aia, Y. Huang, S. Lee, L. Zhang, *J. Alloys Compd.* **2011**, *509*, 2044.

[13] C. Wang, C. Shao, L. Wang, L. Zhang, X. Li, Y. Liu, *J. Colloid Interface Sci.* **2009**, *333*, 242.

[14] H. Cheng, B. Huang, J. Lu, Z. Wang, B. Xu, X. Qin, X. Zhang, Y. Dai, *Phys. Chem. Chem. Phys.* **2010**, *12*, 15468.

[15] Li. El-G, H. Y. Yip, C. Hu, P. K. Wong, *Mater. Res. Bull.* **2011**, *46*, 153.

[16] N. Pugazhenthirana, P. Sathishkumar, S. Murugesan, S. Anandan, *Chem. Eng. J.* **2011**, *168*, 1227.

[17] M. Zidan, T. W. Tee, A. H. Abdullah, Z. Zainal, G. J. Kheng, *Int. J. Electrochem. Sci.* **2001**, *6*, 289.

[18] V. Vivier, A. Régis, G. Sagon, J.-Y. Nedelec, L. T. Yu, C. C. Vivier, *Electrochim. Acta* **2001**, *46*, 907.

[19] V. Fruth, M. Popa, D. Berger, R. Ramer, M. Gartner, A. Ciulei, M. Zaharescu, *J. Eur. Ceram. Soc.* **2005**, *25*, 2171.

[20] M. Gotić, S. Popović, S. Musić, *Mater. Lett.* **2007**, *61*, 709.

[21] M. Ma, J. Zhu, R. Sun, Y. Zhu, *Mater. Lett.* **2010**, *64*, 1524.

[22] A. J. Salazar-Pérez, M. A. Camacho-López, R. A. Morales-Luckie, V. Sánchez-Mendieta, F. Ureña-Núñez, J. Arenas-Alatorre, *Superficies y Vacío* **2005**, *18*, 4.

[23] X. Shen, S. Wu, H. Zhao, Q. Liu, *Phys. E* **2007**, *39*, 133.

[24] K. Laurent, G. Y. Wang, S. Tusseau-Nenez, Y. Leprince-Wang, *Solid State Ionics* **2008**, *178*, 1735.

[25] A. Helfen, S. Merkourakis, G. Wang, M. G. Walls, E. Roy, K. Yu-Zhang, Y. Leprince-Wang, *Solid State Ionics* **2005**, *176*, 629.

[26] T. P. Gujar, V. R. Shinde, C. D. Lokhande, S. Han, *J. Power Sour.* **2006**, *161*, 1479.

[27] E. W. Bohannan, C. C. Jaynes, M. G. Shumsky, J. K. Barton, J. A. Switzer, *Solid State Ionics* **2000**, *131*, 97.

[28] I. Zhitomirsky, *Adv. Colloid Interface Sci.* **2002**, *97*, 279.

[29] T. P. Gujar, V. R. Shinde, C. D. Lokhande, R. S. Mane, S. Han, *Appl. Surf. Sci.* **2006**, *252*, 2747.

[30] I. Valsiûnas, L. Gudavièiûtë, A. Steponavièius, *Chemija* **2005**, *16*, 21.

[31] M. Zdujić, D. Poleti, Č. Jovalekić, Lj. Karanović, *J. Serb. Chem. Soc.* **2009**, *74*, 1401.

[32] B. Ling, X. W. Sun, J. L. Zhao, Y. Q. Shen, Z. L. Dong, L. D. Sun, S. F. Li, S. Zhang, *J. Nanosci. Nanotechnol.* **2010**, *10*, 8322.

[33] H. Zhang, J. Wu, Z. Wang, D. Zhang, *J. Chem. Technol. Biotechnol.* **2010**, *85*, 1436.

[34] H. Zollinger, "Color Chemistry: Syntheses, Properties, and Applications of Organic Dyes and Pigments", Wiley-VCH, Weinheim **2003**, p. 15.

[35] E.-S. Z. El-Ashtoukhy, N. K. Amin, *J. Hazard. Mater.* **2010**, *179*, 113.

[36] H. Olvera-Vargas, N. Oturan, M. A. Oturan, in *"Recent Advances in Energy, Environment and Economic Development,"* S. Eslamian, Editor, Proceedings of the 3rd International Conference on Development, Energy, Environment, Economics, 2012, 99, Paris.

[37] A. I. del Río, J. Fernández, J. Molina, J. Bonastre, F. Cases, *Desalination* **2011**, *273*, 428.

[38] N. Khalfaoui, H. Boutoumi, H. Khalaf, N. Oturan, M. A. Oturan, *Curr. Org. Chem.* **2012**, *16*, 2083.

[39] N. R. De León, K. Cruz-González, O. Torres-López, A. H. Ramírez, J. Guzmán-Mar, C. Martínez-Huitle, J. M. Peralta-Hernández, *ECS Trans.* **2009**, *20*, 283.

[40] A. Rezaee, M. T. Ghaneian, S. J. Hashemian, G. Moussavi, A. Khavanin, G. Ghanizadeh, *J. Appl. Sci.* **2008**, *8*, 1108.

[41] F. Banat, S. Al-Asheh, M. Al-Rawashedeh, M. Nusair, *Desalination* **2005**, *81*, 225.

[42] A. I. del Río, J. Molina, J. Bonastre, F. Cases, *J. Hazard. Mater.* **2009**, *172*, 187.